Solid Freeform Fabrication 2023: Proceedings of the 34th Annual International Solid Freeform Fabrication Symposium – An Additive Manufacturing Conference
Reviewed Paper

Assessing the Impact of the Powder Production Method on Ceramic-filled Polyamide Composites made by Laser Sintering

I. Kletetzka*, F. Neitzel*, H.-J. Schmid*

* Direct Manufacturing Research Center (DMRC) and Particle Technology Group, Paderborn University, Germany

Abstract

Polymer composites represent the industry standard in injection molding for the production of plastic components with increased requirements in terms of heat resistance and stiffness. In the field of laser sintering (LS), these materials are less common so far. In order to extend the available material variety for the LS process, new ceramic-filled Polyamide 613 powders are investigated within the scope of this work. Here, the resulting properties from two different powder production methods are compared. One filled powder is produced by dry blending and the other powder with the same filler and filling ratio is produced by encapsulating the filler particles inside the polymer particles within the dissolution-precipitation process. It was found that encapsulating the filler particles can provide certain benefits for the processability, for example an improved powder flowability or better filler dispersion. However, encapsulating the filler also alters the thermal properties of the precipitated powder.

Introduction

Laser sintering (LS) is an additive manufacturing technology that uses a laser to selectively fuse small polymer particles into solid 3D objects. To do this, the polymer powder is deposited in thin layers on the build platform, preheated by IR heaters to just below the melting temperature, and finally fused by the laser according to the component cross-section. Then the build platform is lowered by one layer height, which is typically around 100 µm. These four steps are repeated until the parts are finished [1–3]. Laser sintering has evolved from a rapid prototyping technology to a process for the direct production of complex plastic components, since it allows the production of complex geometries without the need for support structures and provides a good combination of productivity and detail resolution compared to most other additive manufacturing technologies for thermoplastic materials [3, 4].

For producing functional prototypes or final components, the functional and mechanical properties of additively manufactured parts have become increasingly important [5, 6]. However, the limited selection of LS materials currently available restricts the ability to meet all customer-specific requirements. A survey carried out by Sculpteo reveals that more than 50 % of the participants think that 3D printing needs a wider selection of materials to keep growing (see figure 1). When selecting a material for additive manufacturing 72 % of the participants consider the mechanical properties of the material to be very important. Furthermore, a low material price (52 %) and easy to use materials (44 %) are important to users of additive manufacturing. [7]

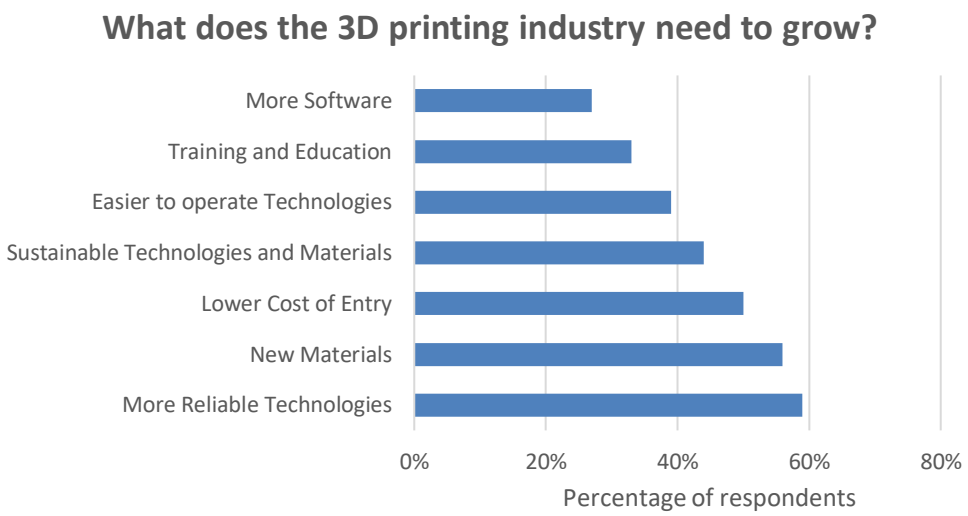

Figure 1: Survey on the influencing factors which limit the growth of 3D printing [7]

Material properties of plastic components can be influenced not only by using different polymers but also by adding fillers to the polymer to create a compound. In the injection molding industry, filled polymers represent the industry standard for components with increased requirements regarding heat resistance and component stiffness. Filled or reinforced polymers are therefore often used in the automotive industry [8]. By adding fillers to laser sintering polymers, the part stiffness, heat resistance and abrasion resistance can potentially be improved while reducing the material cost at the same time [9–12]. Furthermore, flame retardancy or conductivity of polymers can be altered by adding functional fillers [13–15]. Despite these potential advantages, filled materials are rarely used in laser sintering compared to injection molding.

The aim of this paper is to assess the impact of the powder production method on the processability of ceramic-sphere-filled polyamide 613 powder and on the resulting composite properties made by laser sintering. While ceramic-filled LS materials have shown promise in improving mechanical properties [16], their use in industry is still limited. Within the study a dry blended powder will be compared to a powder where the filler particles are encapsulated within the polymer particles. The overall objective is to increase the range of available materials for laser sintering and to create a better understanding of the impact of different production methods of polymer composite powder.

Powder Production Methods

In order to produce polymer powders with fillers for the LS process, there are essentially three different methods suggested by researchers in this field. These are dry blending, melt mixing and encapsulating as illustrated by figure 2.

Dry blending is the fastest and easiest way to produce filled powders for laser sintering. In this process, a polymer powder is mixed with filler particles, e.g. with a drum hoop mixer or a rotary mixer. Various authors use mixing times in the range of 15 min to 24 h [17–19]. Dry blending

requires both the polymer and the filler to already be in powder form with a size suitable for laser sintering (preferably about 20 - 80 µm [1, 18, 20]). Depending on the particle size, particle morphology and densities of the polymer and filler, it may be difficult to achieve a homogeneous mixture [21]. After the mixing process, the powder is typically left in the feed tanks of the LS system for at least a few hours to allow the electrostatic charges generated during mixing to dissipate. The advantage of dry blending is that commercially available plastic powder can be quickly mixed with various fillers and filling ratios, allowing the material to be customized for specific build jobs. A possible disadvantage is that agglomeration or segregation effects may occur depending on the differences in particle size and density between filler and polymer particles. In addition, the adhesion of filler particles and the polymer matrix is based solely on pressure and not on coalescence in the build process [22].

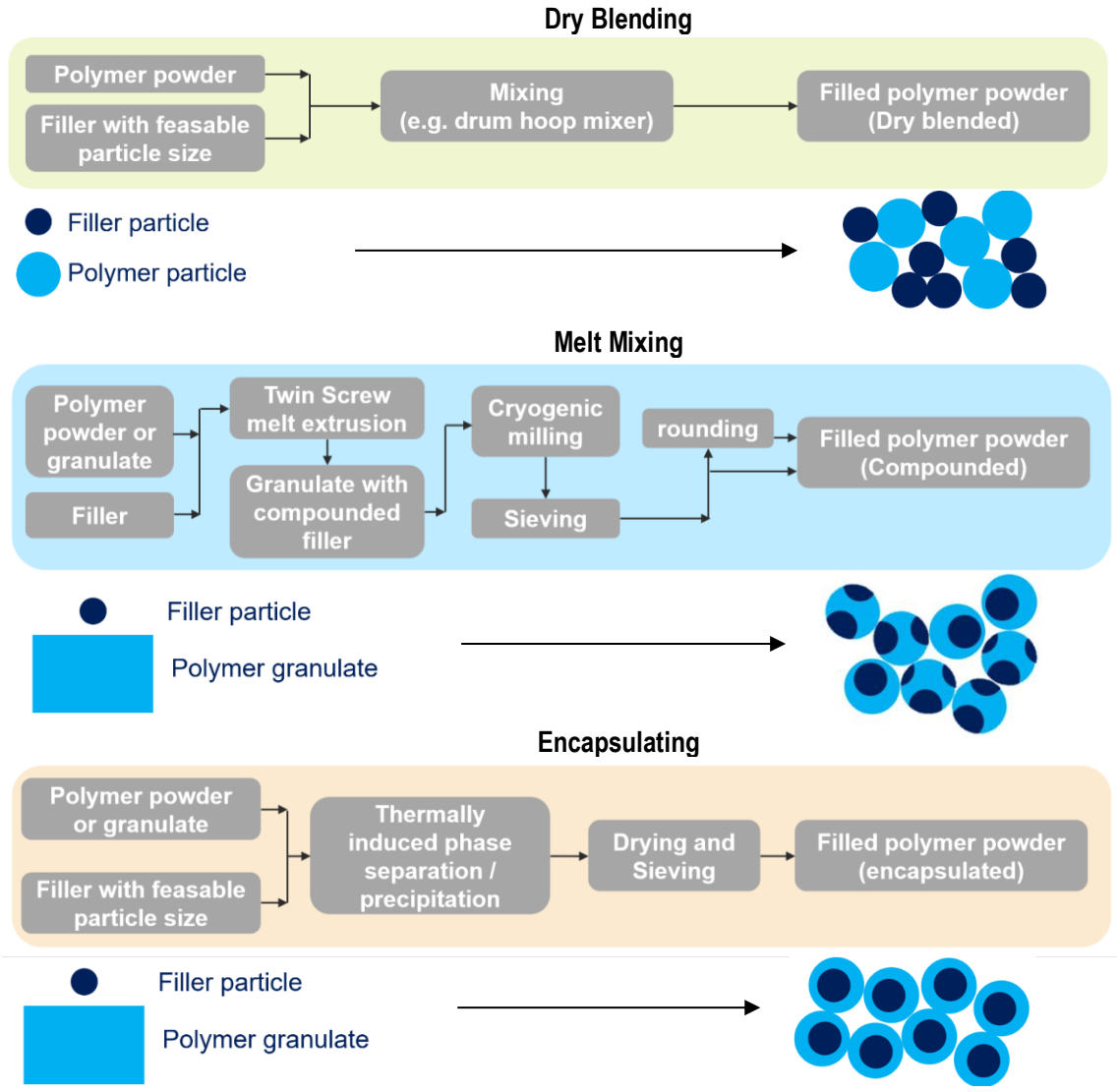

Figure 2: Powder production methods for filled laser sintering materials

Compounding and subsequent cryogenic grinding is another option for the production of filled polymer powders. This process route is referred to as melt mixing in figure 2. In this process, the starting materials do not have to be in powder form. The polymer granules or powder are compounded with the filler in a twin-screw extruder. The resulting compound pellets are then cooled with liquid nitrogen and ground to powder. Since grinding usually results in a particle size distribution that is too broad, the coarse particles are separated by sieving or other classification methods and returned to the mill. In some cases, it is also necessary to remove fine particles from the final product, as these affect the flowability of the powder. The milled powder usually has an irregular shape with sharp edges, which limits the flowability of the powder and therefore negatively impacts the processability [23, 24]. Further rounding steps can improve the flowability of the powder [3]. The mechanisms of particle rounding can be divided into thermal, thermomechanical, mechanical, and chemical, depending on the mode of action. The advantages of this manufacturing process lie, on the one hand, in the flexibility with regard to the materials to be processed and, on the other hand, in the fact that the resulting particles usually contain both filler and plastic. This prevents segregation and may reduce health concerns associated with loose short fibers. In addition, there could be advantages in terms of homogeneity of distribution of the particles in the matrix and in terms of coalescence [25].

The method used in this work to produce particles with incorporated filler particles is to coat the filler particles with a polymer coating within the precipitation process. Either plastic granules or plastic powder can be used for the precipitation process. However, the particle size and shape of the filler particles must be within certain limits, since the filler is not ground in the process and the morphology of the filler particles has a considerable influence on the size and shape of the particles produced in the precipitation process. Unfilled standard polyamide 12 powder is usually produced in a precipitation process from ethanolic solution. The PA12 is dissolved in ethanol under pressure at high temperatures (> 140 °C) and the solution is then cooled slowly and in a controlled manner. Precipitation of the PA12 from the oversaturated solution is initiated by withdrawing the organic solvent and cooling the reactor. The particle size depends on the stirring speed in the reactor [3, 26, 27]. If a dispersed filler material is present in the solvent during the precipitation process, the filler acts as a heterogeneous nucleating agent for the polymer molecules. Therefore, the filler particles are encapsulated in the resulting powder particles. The filler particles have an influence on the crystallization process and can therefore affect the thermal properties of the resulting powder. The advantage of this powder production method is similar to the potential advantages of melt blending: the filler particles are incorporated into the polymer particles. Therefore, a good dispersion of the filler can be achieved and no segregation should occur [28, 29]. In addition, the precipitation process can produce powders with good sphericity and flowability, which are economical for the production of PA12. A disadvantage is the intensive use of solvents and the necessary know-how and careful process control to obtain particles with the desired properties [10].

As can be seen from the sources listed, some research work has already been put into the development of polymer powders with fillers. Most publications concern dry blended powders. In particular, a systematic comparison of the powder properties of powders with incorporated filler particles to a dry blend consisting of the same ingredients is missing so far. Therefore, the aim of this investigation is to compare a dry blended and encapsulated PA613 based LS powder with the same formulation to analyze the advantages and disadvantages of each powder production method.

Materials

The materials for this project were provided by Evonik and are based on their VESTOSINT 3D 8754HT1 PA613 powder. Standard, neat PA613 powder is created by a dissolution precipitation process, similar to standard PA12 powder but can provide better heat resistance and mechanical properties compared to PA12 [30]. In order to further increase the stiffness and heat resistance of the material, ceramic spheres with a mean particle size of 30 µm were added as a filler material. Two different powders with the same formulation were produced by dry blending and by encapsulating the filler particles inside of the polymer particles in the precipitation process. For both material 35 wt% of ceramic spheres were added to the matrix polymer.

The dry blend was created by simply mixing the neat PA613 powder with ceramic spheres in a mechanical mixer. The powder with encapsulated filler particles was produced by using the dissolution precipitation process. First PA613 was dissolved in heated organic solvent. The ceramic beads were dispersed in the solution by stirring. Afterwards the PA613 was precipitated from the solvent. Herby, the ceramic filler particles act as heterogenous nuclei and are therefore coated by the polymer.

Experimental Methods

At first, the powder properties of neat PA613 powder, filled dry blended PA613 powder and filled PA613 powder with encapsulated ceramic spheres are investigated. Particle size distribution, morphology, powder flowability and thermal properties are analyzed to compare the suitability of these powder for use in laser sintering.

For analyzing the **particle morphology**, a Phenom World scanning electron microscope was used, which allows a maximum magnification of up to 24,000 times. In order to create sufficient conductivity of the samples, the samples were sputtered before imaging.

A QICPIC cam sizer manufactured by Sympatec was utilized to determine the **particle size distribution** in compliance with the ISO 13322-2 standard. A RODOS dry dispersion unit and a VIBRI powder feeder were used for dispersion. The measuring range is set to M5, theoretically allowing a detection of particles in the range of 1.8 µm and 3755 µm. [31, 32]

The Hausner Ratio as defined in VDI 3405 Sheet 1.1 is used to determine the **powder flowability.** The Hausner Ratio is defined as the quotient bulk density and tapped density of the powder. Before testing, the powder was deagglomerated and then 250 ml of powder were filled into a measuring cylinder. The measuring cylinder was closed afterwards and tapped uniformly onto a solid surface. The tapping was repeated, until no more compaction and therefore reduction of the powder volume occurred. The Hausner ratio was calculated by dividing 250 ml by the volume, that the powder had after compacting it by tapping. The test is repeated three times and the mean value and standard deviation are given. [33]

In order to ensure that the correct ratio of ceramic spheres was added to the dry blended and encapsulated material and to check if segregation effects occurred, an **ash residue analysis** according to DIN EN ISO 3451-1 method A is carried out. For this purpose, a small sample of

powder or composite part is taken and placed in a crucible inside a Phoenix muffle furnace from CEM at 625 °C for 60 min. After complete ashing of the organic constituents, which in this case is the matrix polymer, the crucible with the sample is cooled to room temperature and the remaining filler is weight to determine the filling ratio.

The **thermal processing window** of the different powders was analyzed by differential scanning calorimetry (DSC) with a DSC 214 Polyma from Netzsch. In accordance with DIN EN ISO 11357-3, powder samples with a mass of 5 mg were heated and subsequently cooled down in an aluminum sample pan. Herby, the heat flow between the sample and an empty reference pan was monitored to identify the melting and recrystallization temperature of the material. During the investigations, the samples were heated up to 280 °C at a heating and cooling rate of 10 K/min. After the first heating and cooling cycle a second cycle was used to compare the materials independent of the thermal history of the different powder production processes. [34]

After characterizing the important properties of the different powders, the materials were processed on an EOS P396 laser sintering system. Suitable laser parameters for unfilled PA613 are known from previous investigations [16, 30]. The parameters were adapted for the filled variants by varying the laser power and additionally testing double exposure strategies for optimized coalescence. Suitable laser parameters were identified by analyzing the mechanical properties and part resolution for different parameters. The selected build parameters are given by table 1.

Table 1: Build parameters for investigated powders

Parameter	Neat PA613	Dry blended PA613	Encapsulated PA613
Layer height [µm]	120	120	120
Temperature			
Build chamber [°C]	206.5	206.5	188
Removal chamber [°C]	140	140	140
Global beam offset [mm]	0.32	0.32	0.32
Hatch (Hatch exposure 1 / Hatch exposure 2)			
Laser power [W]	38 / -	26 / 26	26 / 26
Scan Speed [mm/s]	4750	4750	4750
Hatch distance [mm]	0.25	0.25	0.25
Offset [mm]	0.3	0.3	0.3
Contour (contour line 1 / contour line 2)			
Laser power [W]	24 / 24	24 / 20	24 / 20
Scan speed [mm/s]	3000	3000	3000
Offset [mm]	0.15 / 0	0.15 / 0	0.15 / 0

After determining suitable parameters, test specimens were built from all three powder and characterized. Tensile tests, compression tests and heat resistance tests were carried out. Additionally, the parts were analyzed by computer tomography (CT).

The mechanical properties of polyamides are strongly dependent on the moisture content in the material, therefore a precise adjustment of this value is necessary to obtain repeatable

measurements. As stated by DIN EN ISO 1110, the mechanical properties of polyamides should be tested after performing an **accelerated conditioning process** to ensure they have reached the equilibrium moisture level, that would occur after several years of use in standard climate conditions. Therefore, specimens were stored in a climate chamber at 70°C and 62 % relative humidity for 168 h. After conditioning in the climate chamber, the specimens were kept at standard climate conditions (23°C 50 % relative humidity) for a minimum of 72 h before mechanical tests were carried out. In addition to the tests in conditioned state, specimens were tested in dry state. They were therefore kept in closed plastic bags together with silica pads to prevent moisture absorption before testing. [35]

Tensile tests were carried out as described in DIN EN ISO 527. Sample geometry 1A was used and tested on an Instron 5569 universal testing machine with a 5 kN load cell. The test speed for determining the modulus of elasticity is 1 mm/min and is then increased at 0.27 % elongation until fracture. In accordance with the material standard for polyamides, unreinforced samples were tested at 50 mm/min and filled materials are tested at 5 mm/min. For every parameter set, average mechanical properties were calculated using 5 test specimens and standard deviations are given. The pre-load for all tests was 0.1 MPa with activated specimen protection. It is indicated in each case whether the samples were tested in the dry or conditioned state. [36, 37]

The mechanical properties under compressive loads may differ from those under tensile loads. Fillers in particular can cause this effect. Therefore, the **modulus for compression loads** is determined additionally to the tensile values. The compressive modulus is determined according to DIN EN ISO 604. For the compression tests an INSTRON 5569 universal testing machine with a 5 kN load is used. For the compression modulus measurement, the strain is recorded optically. The test speed is 1 mm/min. Unless otherwise stated, 5 samples are tested at a time and mean and standard deviation are given. It is indicated in each case whether the samples were tested in the dry or conditioned state. [38]

As one of the project goals was to increase the heat resistance of the material, the **heat deflection temperature** is measured according to DIN EN ISO 75 method A. Test specimens with dimensions 80 × 10 × 4 mm are used in the flat lying test position. The HDT value is calculated as an average from three test specimens and the standard deviation is given with error bars. [39, 40]

Powder Characterization and Processability

The particle size distribution (PSD) and particle morphology dictate the powder flowability and the powder bed density and therefore have a strong impact on the quality of LS parts. Poor flowability can lead to recoating errors and a low powder bed density can decrease mechanical properties. The particle size distribution impacts the surface quality and limits the lowest possible layer height within the process as well. Finer particles can improve the surface quality but limit powder flowability. Spherical particles are desirable for best powder flowability and powder bed density. [3]

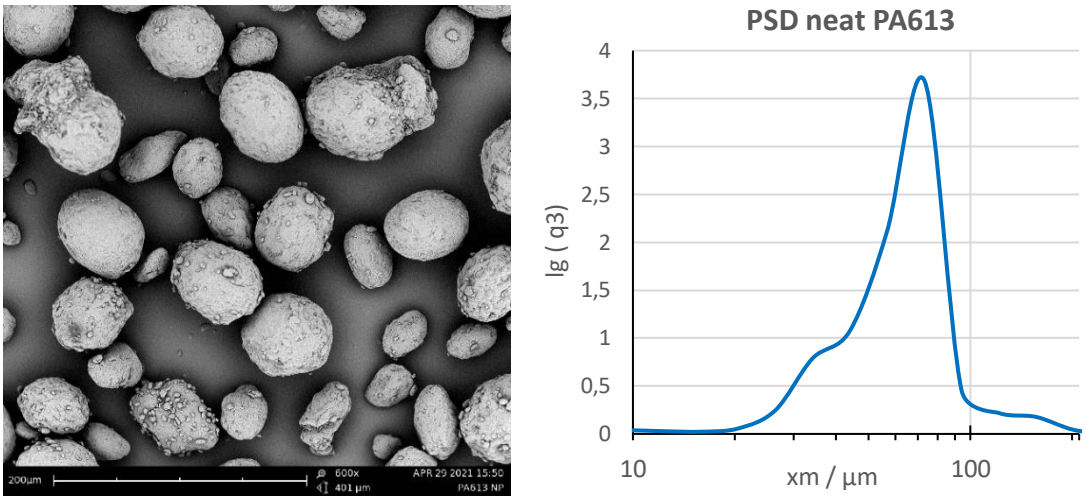

Figure 3: SEM image neat PA613 virgin powder (left) and PSD (right)

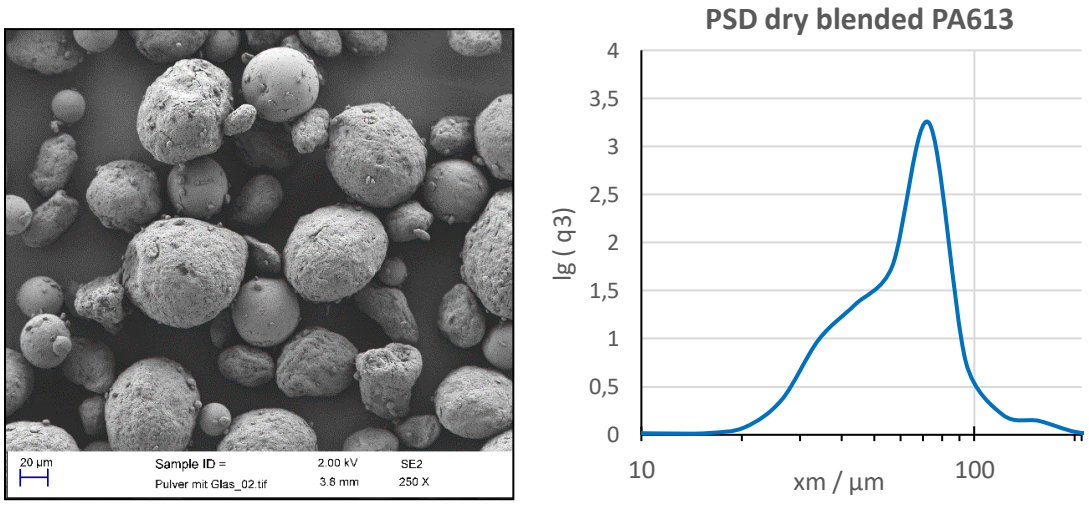

Figure 4: SEM image PA613 dry blended with ceramic filler (left) and PSD (right)

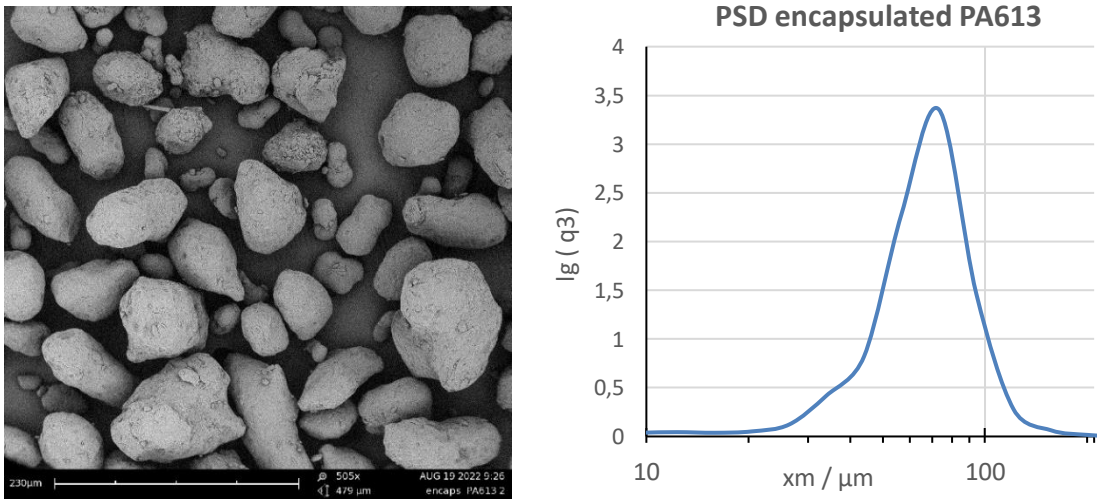

Figure 5: SEM image PA613 with encapsulated ceramic filler (left) and PSD (right)

Neat VESTOSINT 3D 8754HT1 PA613 polymer powder has a regular potato shaped morphology, as shown in figure 3 on the left. Some smaller sub particles adhere to the particle surface. The average sphericity of the particles is ØΨ = 0.852. The particle morphology is typical for a precipitation process and seems well suited for processing in laser sintering. The particle size distribution is shown on the right and is typical for laser sintering powder. There are some larger particles in the material, so layer heights below 100 µm would not be advisable. The d_{10}, d_{50} and d_{90} values are given in table 2.

Figure 3 shows the PA613 powder dry blended with ceramic beads. The polymer particles and the ceramic beads can be clearly distinguished in the SEM image. The ceramic beads have a very high sphericity, a smooth surface and are smaller compared to the PA613 powder (see d_{50} values in table 2). The mixed powder therefore has a higher proportion of fine particles compared to neat PA613 powder.

The particle morphology of the PA613 powder with encapsulated ceramic beads is shown in figure 4. In contrast to the dry blend, the filler particles cannot be seen. This indicates that the ceramic beads are well embedded into the base polymer. The particles have more of an edgy particle shape compared to neat PA613. The sphericity of the encapsulated powder ØΨ = 0.832 is slightly lower compared to the neat PA613 ØΨ = 0.852. Compared to powder produced by cryogenic grinding, the particle morphology is still better suited for laser sintering, since the particles have smooth surfaces, and the sphericity is only slightly lower compared to standard neat PA613. There are a few fine powder particles visible that potentially do not have any ceramic particles embedded inside. The particle size of the powder with encapsulated ceramic beads is similar to neat PA613 and therefore suitable for laser sintering.

The actual filling ratios of both powders was determined by performing an ash residue analysis. The results are listed in table 2. The volume averaged outer radius of the encapsulated powder r_a can be calculated from the volume share of filler v_f and the radius of the filler particles r_f, assuming a homogeneous filler distribution as well as spherical particles (equation 1).

$$r_a = r_f * \sqrt[3]{\frac{1}{v_f}} \tag{1}$$

Using this equation and the powder characterization results, the mean particle size of the encapsulated powder can be calculated as 66.8 µm. Under the given assumptions, this value shows good agreement with the measured median value of 68.0 µm.

Table 2: Comparison of sizes distributions, sphericity and filling ratio

	d_{10} (µm)	d_{50} (µm)	d_{90} (µm)	Average sphericity ØΨ	Filling ratio vol%
Neat PA613 (unfilled)	34,48	64,57	82,87	0,852	0
Dry blended PA613 ceramic filler	32,98	63,19	90,50	0,851	8,25
Encapsulated PA613 ceramic filler	40,38	68,00	98,07	0,832	9,52
Ceramic filler after ashing	15,87	30,48	52,50	0,899	-

Bulk density, tapped density and the Hausner ratio are determined for all three powder variations. The results are given by figure 6. As expected, the bulk density and the tapped density of the filled materials is higher compared to neat PA613 since the density of the ceramic filler (6 g/cm³) and glass (2.5 g/cm³) is higher than that of neat PA613 (1.04 g/cm³).

Neat PA613 has a Hausner ratio of around Hr = 1.2. Powders with a Hausner ratio below 1.25 are classified as having good flowability. Above 1.25, powder flowability is classified as limited and above 1.4 cohesion dominates. The encapsulated material exhibited an even better flowability with Hr = 1.15 compared to neat PA613 even though the particle morphology was a bit more edgy. Since the encapsulated material is a "prototype material", it cannot be fully ensured that exactly the same amount of flow aid (nanosilica) is present in the material compared to neat PA613. The higher flowability could be due to the use of more flowing aids. To protect Evonik's intellectual property, the used flow aid cannot be further specified. The Hausner ratio of the equivalent dry blend is Hr = 1.30 and is therefore much higher than that of the encapsulated material. Since the value is above 1.25, the dry blend with ceramic beads is classified as having a reduced flowability. It is known that a higher portion of fine particles can cause worse powder flowability, however this effect is quite extensive in this case. Previous investigations with filled PA613 powder also revealed a worse powder flowability if finer filler particles were added, but the effect was not quite as extensive [16].

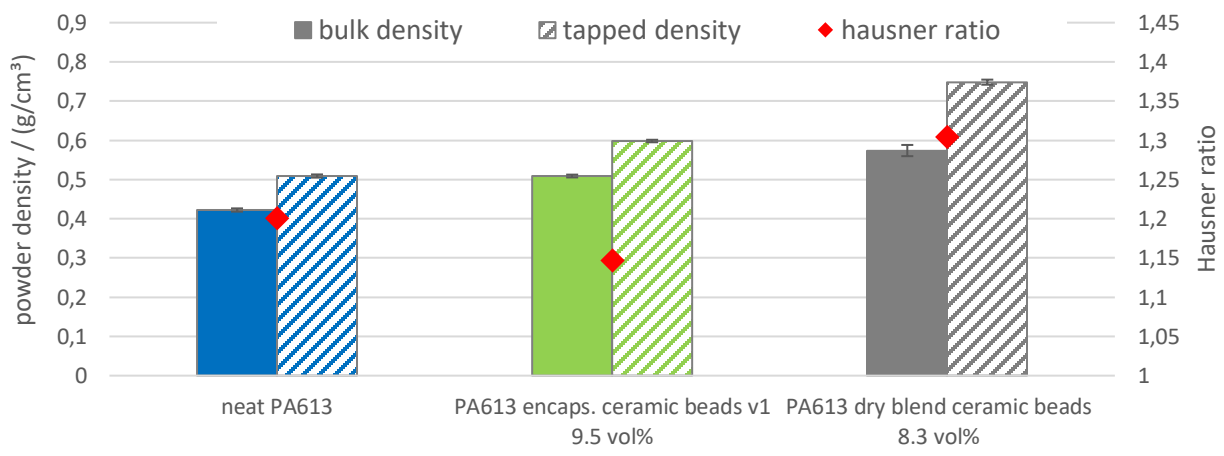

Figure 6: Comparison of Hausner ratios of dry blended and encapsulated powder

The thermal properties of neat PA613, dry blended and the encapsulated material were investigated with DSC measurements in order to identify the sintering window and to analyze differences. The first temperature cycle shows that the neat PA613 has an onset melting temperature of 208.6 °C and a recrystallization onset temperature of 176.4 °C and therefore a wide sintering window (see figure 7). As expected, the dry blended material has a similar melting temperature, since the polymer powder is same, just mixed with fillers. The melting enthalpy is lower since the filler does not melt. During recrystallization of the polymer filler mixture, the filler can act as an heterogenous nuclei and cause recrystallization at higher temperatures [41]. The recrystallisation peak temperature of the dry blend is slightly higher than that of neat PA613.

The encapsulated material exhibits different thermal properties compared to the dry blend. It has a secondary melting peak before the main melting peak at a lower temperature. The filler can

not only act as a nucleus for crystallization for the polymer melt, but also during the dissolution precipitation process. During precipitation, the polymer molecules interact with the filler particles and therefore coat the surface of the filler. This can cause differences in the crystalline structure of the polymer and therefore influence its thermal properties. The secondary melting peak is not desirable for laser sintering. Further investigations showed that with adapted parameters during the precipitation, this secondary peak can be avoided, but the investigations within this work were carried out with the material that showed the secondary peak. Further publications with the optimized material will be released in the future. The encapsulated material also exhibited a higher recrystallization temperature compared to the dry blend. It is assumed that this effect is caused by a higher amount of silica flowing aids present in the encapsulated powder.

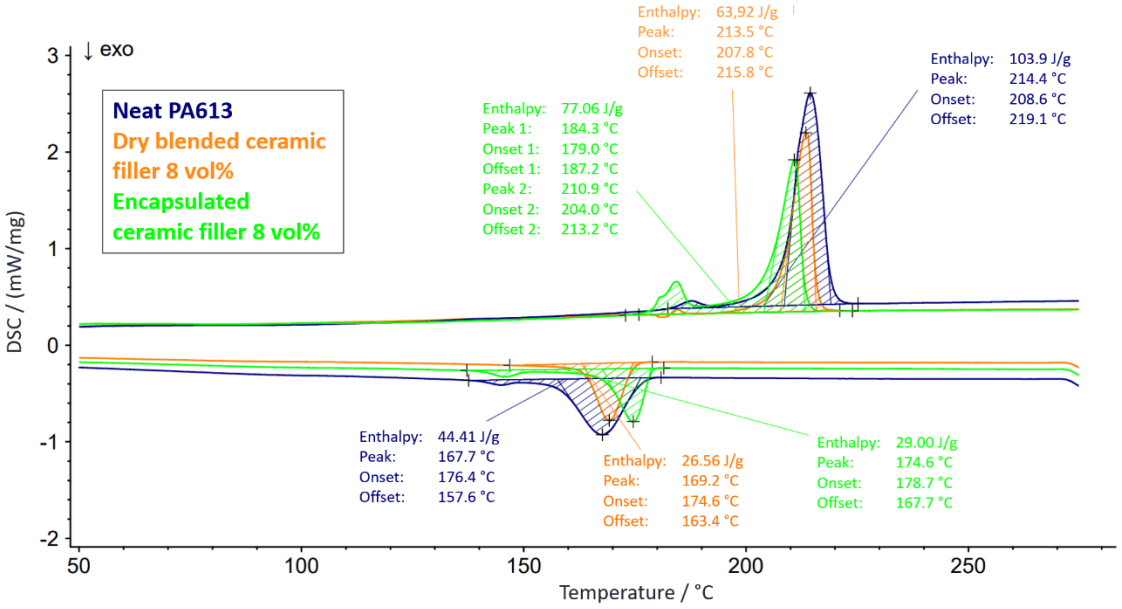

Figure 7: DSC of neat PA613, dry blended and encapsulated variants first temperature cycle

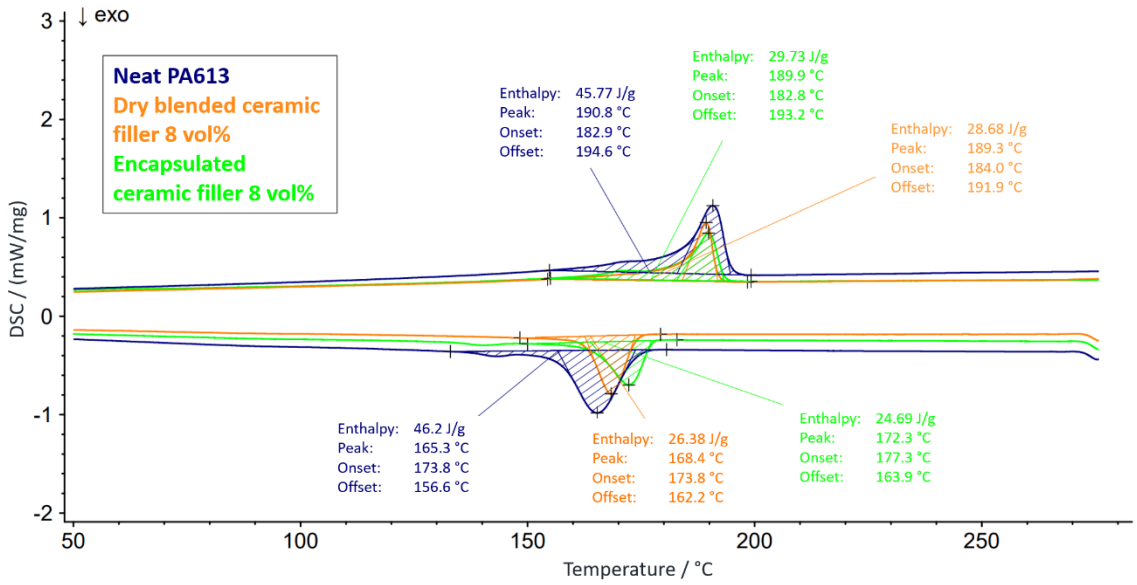

Figure 8: DSC of neat PA613, dry blended and encapsulated variants second temperature cycle

After the first temperature cycle an identical second temperature cycle is measured in the DSC (figure 8). Since the thermal history is erased by melting the material in the first temperature cycle, the encapsulated and the dry blended material should show similar properties. The melting temperature of all materials is lower than in the first cycle and the melting enthalpy is significantly lower. This shows that the crystallinity of the laser sintering powder is higher before melting it once and that the cooling rate in the dissolution precipitation process is apparently lower than the 10 K/min used for the DSC measurements. In the second temperature cycle, the encapsulated and the dry blended material show very similar melting temperatures as one would expect.

For processing the powders on an EOS P396, the powder bed temperature was set by determining the temperature necessary to prevent curling of the parts. For the encapsulated material, a powder bed temperature of 188°C was necessary. This temperature is higher than the peak temperature of the secondary melting peak (184.3°C) that the encapsulated powder exhibited in the DSC measurements. This resulted in very pronounced caking of the powder bed to the point that it was difficult to remove the parts from the powder bed after the build job (figure 9 middle). With some effort, the parts could still be removed from the powder bed and the adhering powder could be removed by glass bead blasting. Surface quality of the parts build with encapsulated powder was good (figure 9 right). For the dry blended material and neat PA613 a powder bed temperature of 206.5 °C was selected to prevent curling. Parts could be built without problems and without severe caking of the powder bed with these powders. Different exposure parameters were tested and the parameters that could provide the best results were selected (table 1). The same exposure parameters were used to build parts from dry blended and encapsulated powder.

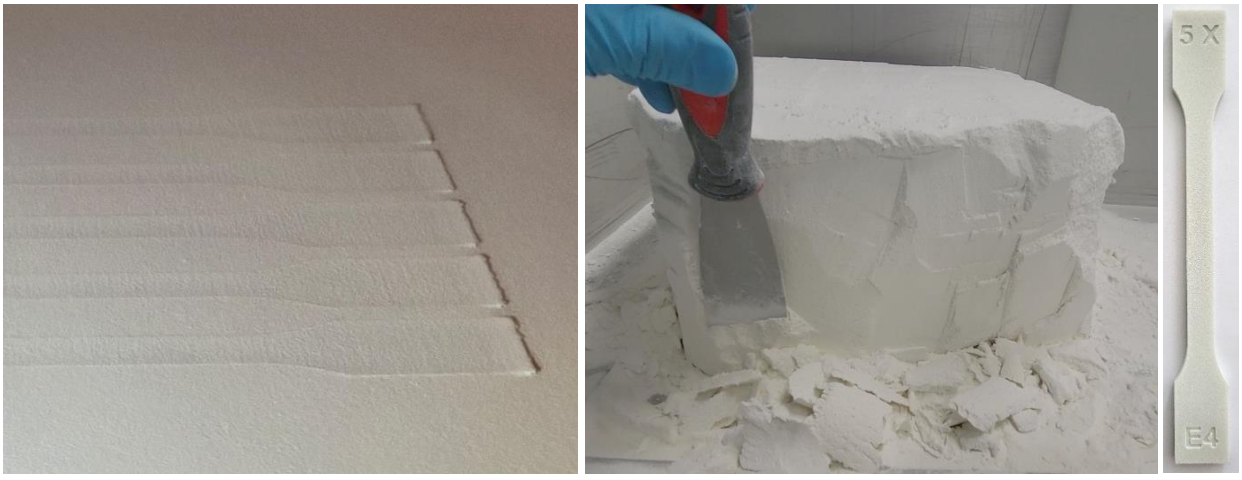

Figure 9: Curling of Specimens at temperatures lower than 188 °C with encapsulated powder (left), pronounced caking of the powder bed with encapsulated powder (middle) and part from encapsulated powder after glass bead blasting (right)

One potential disadvantage of dry blending polymers powders and fillers is that segregation effects could occur inside the powder containers during the build job. The powder containers are usually fluidized with compressed air, to ensure optimal flowability of the powder. In the experiments of this work, the powder was flushed with nitrogen every 3 min for 10 s. If there are

major differences in density or size between the polymer powder and the filler, there is a risk that the individual components will segregate. In the LS process, this effect would mean that the filler content in the components would not remain constant over the height of the build job. Thus, constant material properties could not be guaranteed. To measure possible segregation effects, tensile test specimens built at different heights in the same build job are analyzed by burning out the polymer matrix and determining the filling ratio according to the ash residue method. If the filling ratio is constant over the full height of the build jobs, it can be assumed that no segregation effects occurred. The results for the PA613 powder with encapsulated ceramic spheres, dry blended ceramic spheres and two further PA613 dry blends with glass beads are given in figure 10.

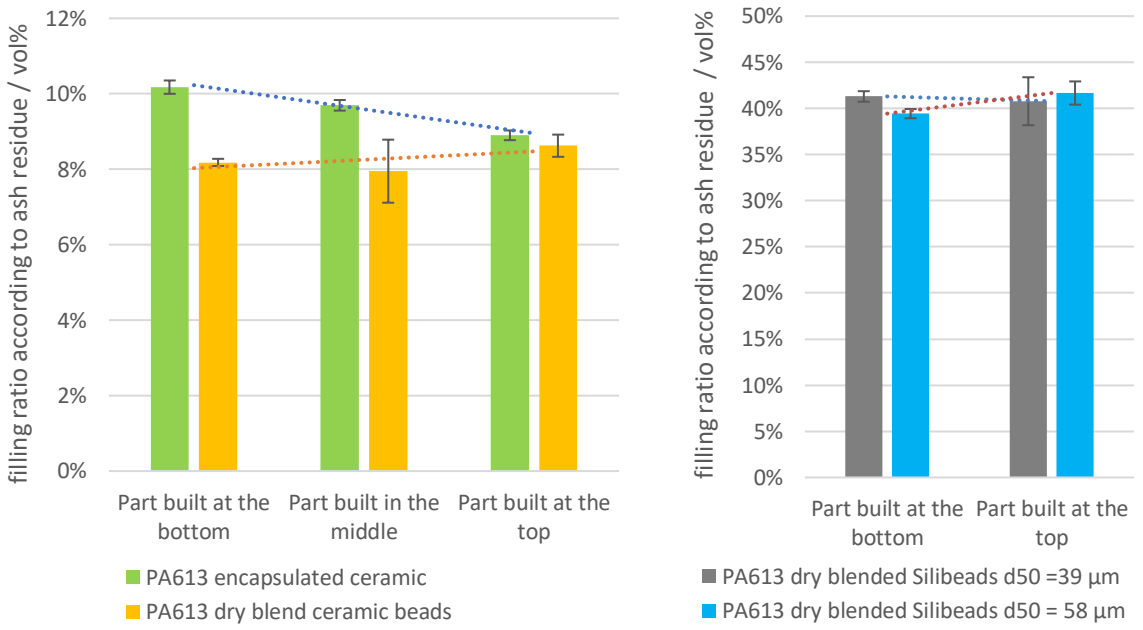

Figure 10: Segregation measured by ash residue analyses of parts built at different built heights for dry blended and encapsulated ceramic filler (left) and dry blended glass beads (right)

The filling ratio is between 8 and 10 vol% for the dry blended and encapsulated ceramic filled powders. Surprisingly, the measured variation of the filling ratio was higher for the encapsulated powder compared to the dry blend. The dry blend showed no significant variation in filling ratio. Also, further investigations with glass bead filled dry blend revealed no significant differences in the filling ratio over the build height. It is therefore deduced that no significant segregation effects occur for dry blends in the feed tanks of an EOS P3 system, if the filler particles are in the range of 30 µm to 60 µm. The encapsulated powder shows a slightly reduced filling ratio towards the top of the build job. Since no segregation occurred in the dry blend and the filler is encapsulated by polymer, no segregation effects should theoretically occur for the encapsulated material either. The encapsulated powder was not mixed after the precipitation process. Therefore, inhomogeneities in the filling ratio from the production process could still be present and cause this effect. For further investigations, the complete batch of precipitated powder will be mixed before processing to rule out this cause of the inhomogeneities.

For analyzing the homogeneity of the filler distribution within the printed parts, CT scans of laser sintered cubes (10 mm x 10 mm x 10 mm) were used. Exemplary sectional views of these scans can be found in figure 11.

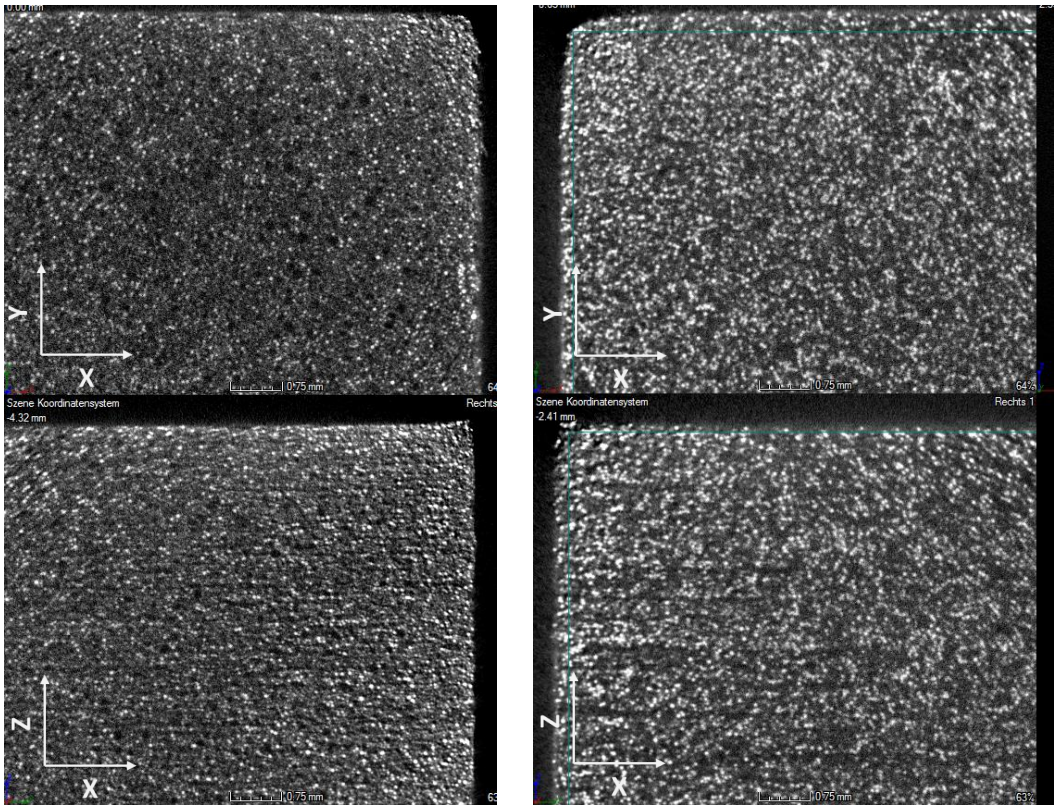

Figure 11: Filler distribution in parts built with encapsulated powder (left) and dry blended powder (right)

Comparing the scans of the encapsulated and dry blended material, some differences can be found. For the dry blended material (figure 11 right), the filler particles often occur in small agglomerates, where a few ceramic beads are in direct contact with each other. Additionally, regions with a lower concentration of filler particles are visible. Here mainly molten PA613 is present. The part seems to have a low porosity for a laser sintered cube.

The ceramic particles in the cube built with the encapsulated material (figure 11 left) seem to be better dispersed. Less agglomerations can be found in the sectional views. However, the part built from the encapsulated material has a much higher porosity (8.9 %) compared to the dry blend (4.9 %). Especially in the middle of the cube of lot of pores can be found. It is assumed that the differences in thermal behavior are the main cause of the porosity. Since the encapsulated material had to be processed at 18.5 K lower part bed temperature, the layers cool down faster after being molten by the laser. On top of that, the encapsulated material has a higher recrystallization temperature, meaning the exposed layers will recrystallize faster. According to the widely used Frenkel-Eshelby model for coalescence of molten particles, the coalescence increases over time the particles are in molten state. The process is faster for particles with a lower melt viscosity and higher surface tension. According to this model the coalescence for the encapsulated powder will

likely be worse and the porosity therefore higher [42–44]. The higher porosity of the parts built from encapsulated powder will most likely have a negative impact on the material properties.

Figure 12 shows the filler distribution within dry blends that have been investigated previously. Here, a higher filling ratio of spherical fillers or the use of glass fibers led to worse agglomerations than observed for the dry blend with ceramic spheres. These investigations showed that the tendency for agglomeration increases with smaller filler particles, higher filling ratios and fillers with higher aspect ratios (fibers). For producing powders with these fillers, encapsulating the filler might provide even bigger benefits regarding the filler matrix distribution compared to the investigated powder with ceramic spheres and a filling ratio of less than 10 vol%. The observed agglomeration for dry blends hindered the successful processing of the materials in figure 12 and encapsulating could be a potential solution for this problem.

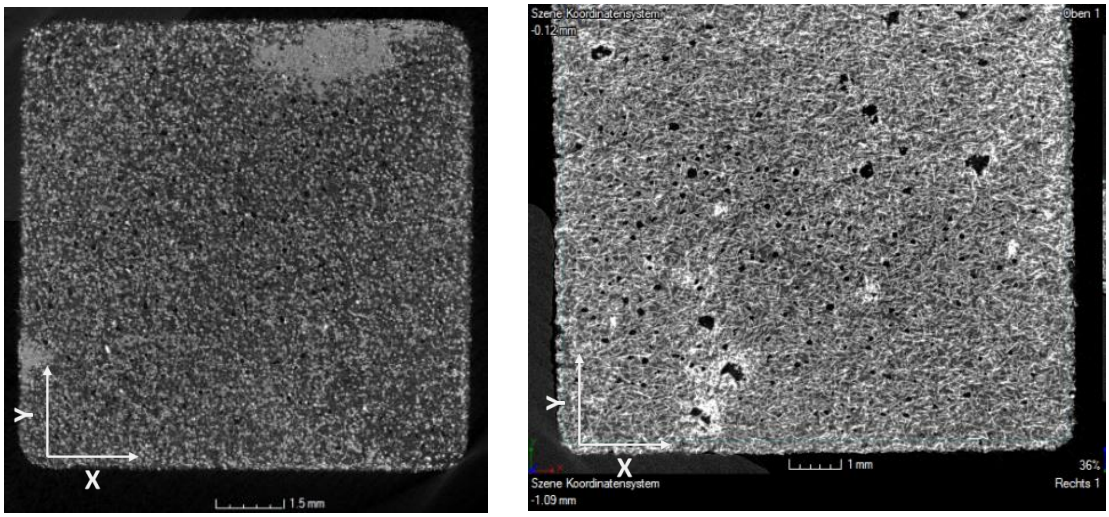

Figure 12: Agglomerate of glass beads in part built from PA613 dry blend with 20 vol% glass beads with a d_{50} of 32 µm (left) and agglomerated glass fibers in dry blended PA613 (right)

Part Properties

Tensile specimens according to DIN EN ISO 527 were built with laser parameter specified in table 1 from neat and filled PA613 powder in X, Y and Z direction and tested in dry state and after an accelerated conditioned procedure according to DIN EN ISO 1110. The results are given by figure 13 to 15.

The dry blend and the material with encapsulated ceramic spheres both provide a similar increase in modulus of about 50 % in the dry state and after conditioning the specimens compared to neat PA613. The tensile strength of the filled material is slightly lower than for the neat material, indicating limited filler matrix adhesion. After conditioning, the difference in tensile strength of neat and filled PA613 is even bigger, indicating a further loss of filler matrix adhesion as previously noticed for glass bead filled PA613 [45]. While the dry blend exhibited isotropic strength properties, reduced properties were observed for the encapsulated material in z-direction. This effect is most likely caused by the lower powder bed temperature and the higher porosity of the

encapsulated material. As expected, the elongation at break of the filled materials is reduced, however the encapsulated material performed again worse in z-direction compared to the dry blend.

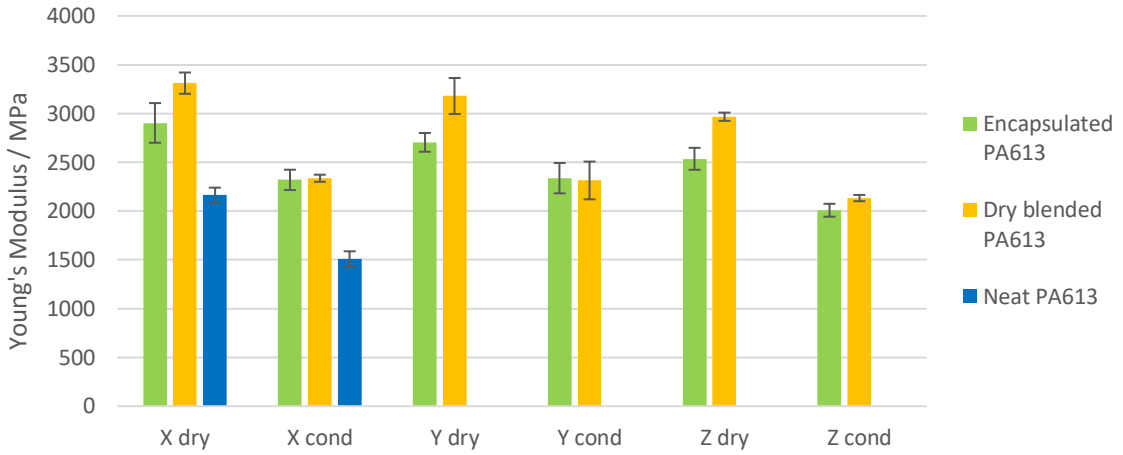

Figure 13: Tensile Modulus for ceramic filled and neat PA613 powder

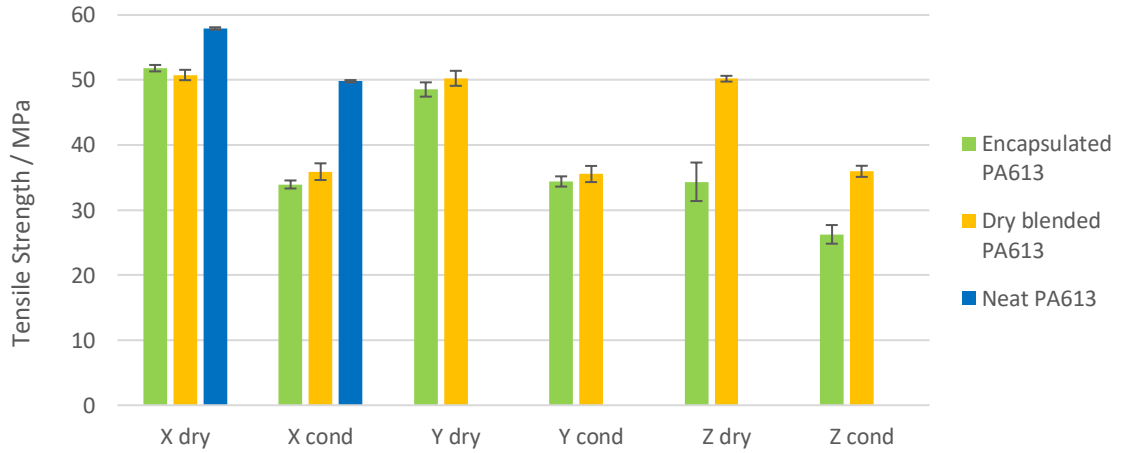

Figure 14: Tensile strength for ceramic filled and neat PA613 powder

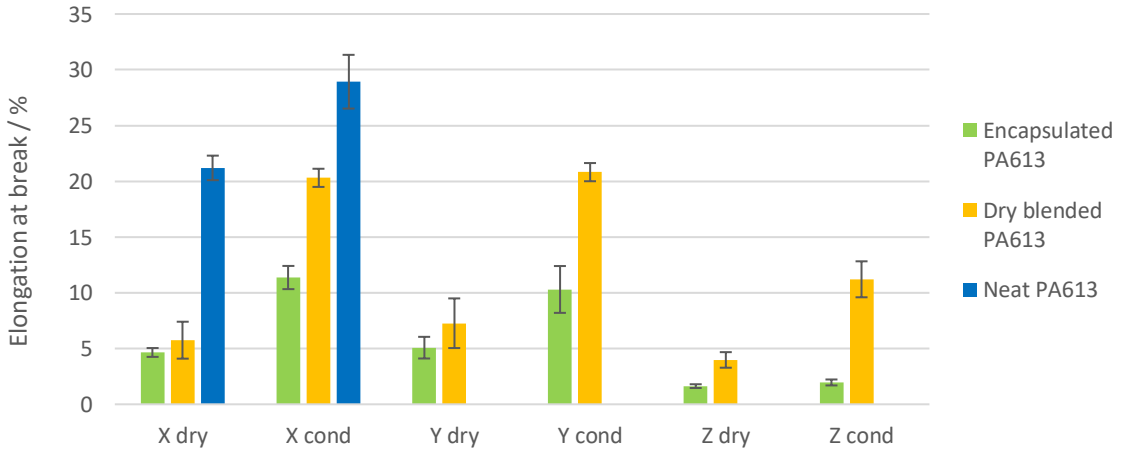

Figure 15: Tensile elongation at break for ceramic filled and neat PA613 powder

Comparing the stress strain curves of the different materials, differences in the linear part of the stress strain curve are noticeable. Figure 16 shows three exemplary stress strain curves of neat PA613, dry blended PA613 and PA613 with encapsulated ceramic filler in conditioned state. For each curve, the stress level that causes a deviation in elongation of 0.2 % compared to the ideal elastic line has been calculated and is visualized. This value will be called $\sigma_{0,2}$ in this report. The deviation from the linear stress strain behavior could theoretically either be caused by slipping of the macro molecules and resulting plastic deformation of the polymer itself or loss in filler matrix adhesion and a resulting reduction in stress in the material at a given elongation. The higher the $\sigma_{0,2}$ value is, the higher loads the material can withstand without showing a large deviation from the ideal linear material behavior. For metals, the $R_{P\,0,2}$ is used if the material has no distinctive yield point in order to calculated the limit of the elastic material behavior [46]. Since polymers are known to have a time dependent viscoelastic material behavior, the $R_{P\,0,2}$ value is not defined for polymers. However, the $\sigma_{0,2}$, which is defined similarly to the $R_{P\,0,2}$ for metals within this report, can still give an indication on stress levels that cause a plastic deformation or damage to the material at the given strain rate that was used for the tensile testing. Even though this method has its limitation for polymers, a larger linear area of the stress strain curve is still desirable. The described method has been used to calculate the $\sigma_{0,2}$ value for neat, dry blended and encapsulated PA613 material in dry and conditioned state. In addition to the mean value for the five tested tensile specimens, the standard deviation is given by figure 16.

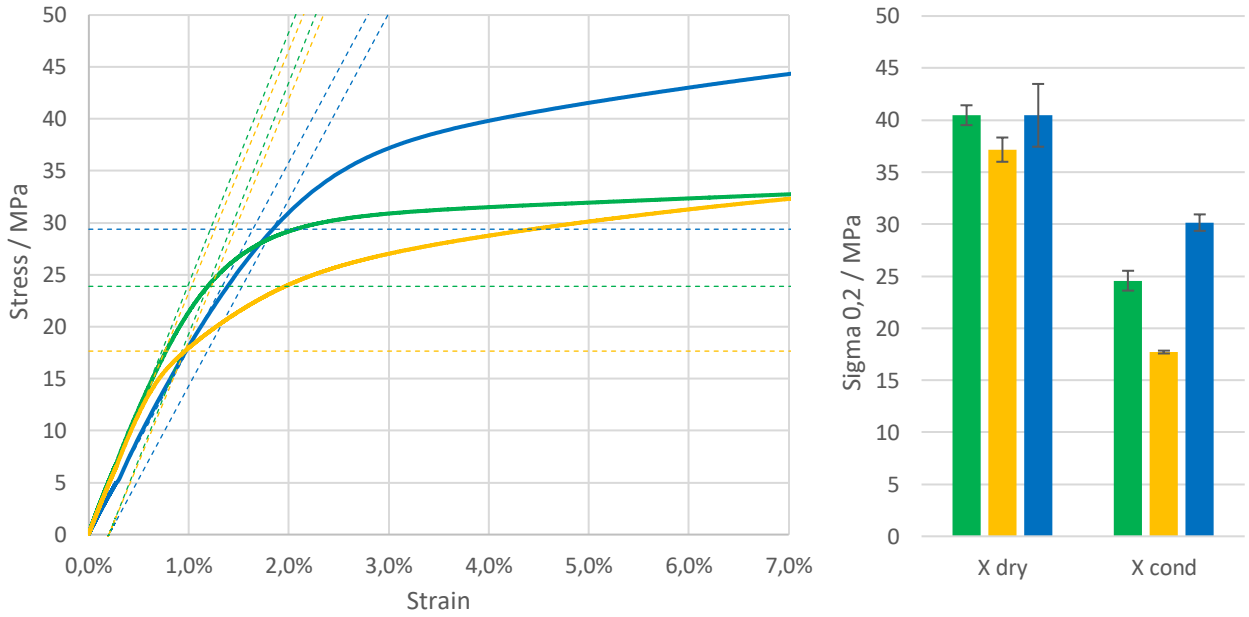

Figure 16: Stress strain diagram of conditioned specimens printed in X-direction (left) and calculated $\sigma_{0,2}$ values for ceramic filled and neat PA613 powder (right)

Even though the encapsulated material exhibited very similar tensile strength and stiffness compared to the dry blend in the conditioned state, there are significant differences visible for the $\sigma_{0,2}$ values. The encapsulated material has a linear material behavior up to higher tensile stress compared to the dry blend. This can be beneficial since these parts can withstand higher loads before experiencing permeant deformation or damage to the material. This is an interesting observation indicating that the filler matrix adhesion in the encapsulated material can transfer

slightly higher forces before failing. At the maximum tensile strength and beyond that, the material still fails due to loss of filler matrix adhesion as is visible by the lowered tensile strength compared to unfilled material.

In addition to the tensile modulus, the compression modulus of the different materials was analyzed (figure 17). It was found, that for compression loads the spherical filler provided an even higher increase in part stiffness. In Z-direction both the dry blended and the encapsulated powder have a higher modulus compared to the XY-plane. Again, the dry blend performed slightly better than the encapsulated material. The porosity found in the encapsulated material will have a negative impact on the compression modulus and can explain the observed difference.

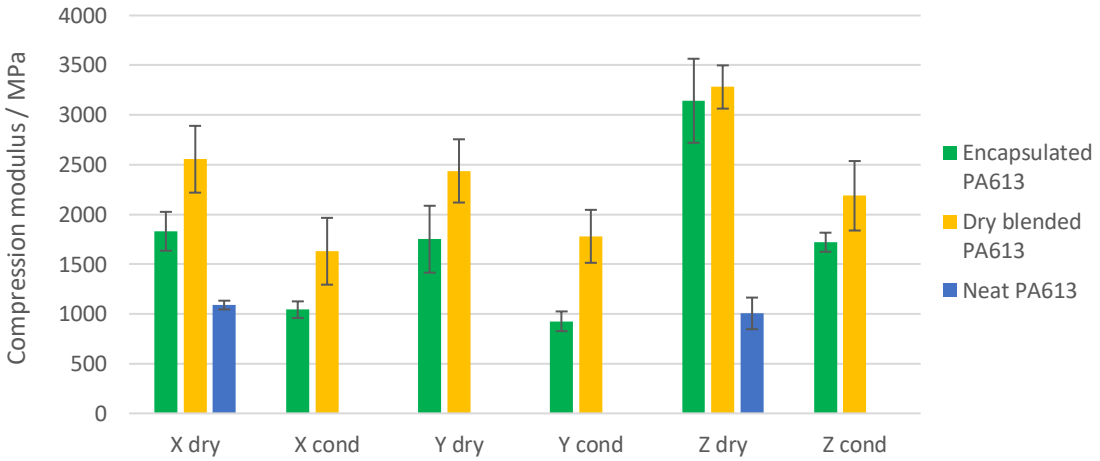

Figure 17: Compression modulus in dry and conditioned state of PA613 with dry blended and encapsulated ceramic spheres

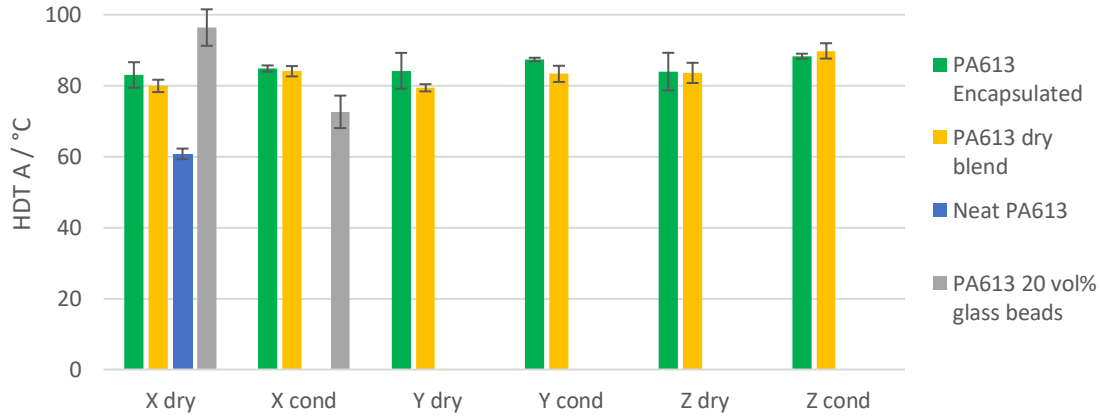

Figure 18: Heat deflection temperatures at 1,8 MPa load of neat and filled PA613 powders

Heat deflection temperature of neat PA613 could be increased by 20 °C with the addition of ceramic spheres to neat PA613. Both the dry blend and the encapsulated material exhibited the same heat resistance. While the heat resistance of glass a bead filled PA613 was reduced after conditioning the specimens, the ceramic filled PA613 showed isotropic heat resistance properties

that were not affected by conditioning. This indicated that the filler matrix adhesion of glass filled PA613 was impacted more severely by conditioning than that of ceramic filled PA613.

Summary and Outlook

Within the scope of this work, two filled PA613 powders for laser sintering were investigated. Both powders consist of PA613 filled with around 35 wt% of ceramic spheres. One powder was produced by dry blending the ceramic spheres with commercially available VESTOSINT 3D 8754HT1 PA613 powder. For the production of the other powder, the ceramic spheres were added during the dissolution precipitation process at Evonik so that the ceramic spheres were coated with AP613 powder and were therefore fully encapsulated.

Analyzing the processability of both powders revealed, that encapsulating the ceramic spheres improved the powder flowability and provided a better dispersion of the filler particles within the polymer matrix. It was found that no segregation of polymer powder and filler occurred in the feed tanks of an EOS P3 system for the dry blend. In this regard, it is not necessary to encapsulate the filler particles. However, segregation effects could still occur in the powder recycling process during sieving. The encapsulated powder exhibited different thermal properties compared to the dry blend. A secondary melting peak before the main melting peak was identified as the cause for severe caking of the powder bed, even though the encapsulated material was processed at 18.5 °C lower powder bed temperature than the dry blend. With adapted processing parameters during the dissolution precipitation, it was possible to produce a new variant of the encapsulated powder that has almost the same thermal properties compared to the dry blend and will be investigated in further detail in the future.

The resulting parts built from PA613 with encapsulated and dry blended ceramic filler have a white appearance with good resolution and surface finish. Compared to neat PA613, both filled powders exhibited a higher tensile and compression modulus and an increased heat deflection temperature. Tensile strength and elongation at break were reduced for the filled powders compared to neat PA613. Some mechanical properties of PA613 with encapsulated ceramic filler were slightly worse than that of the dry blend. Especially in Z-direction the dry blend exhibited superior tensile strength and elongation at break. It is believed that this difference is caused by the higher porosity within the parts built with encapsulated powder. The porosity is most likely the result of the much lower powder bed temperature used to process the encapsulated material and might be improved with the new variant on encapsulated powder that does not show the secondary melting peak. It was found that the encapsulated material exhibits a more linear stress strain behavior than the dry blend. The same stress caused less strain. It is assumed that this improvement is due to a better filler matrix adhesion and/or a better filler dispersion of the encapsulated material. The results for this investigation with PA613 should be easily transferrable to PA12, since this polymer is also produced by a dissolution precipitation process at Evonik.

References

[1] R. D. Goodridge, C. J. Tuck, and R. Hague, "Laser sintering of polyamides and other polymers," *Progress in Materials Science*, vol. 57, no. 2, pp. 229–267, 2012, doi: 10.1016/j.pmatsci.2011.04.001.

[2] J. Breuninger, R. Becker, A. Wolf, S. Rommel, and A. Verl, *Generative Fertigung mit Kunststoffen*. Berlin, Heidelberg: Springer Berlin Heidelberg, 2013.

[3] M. Schmid, *Lasersintern (LS) mit Kunststoffen*. München: Carl Hanser Verlag GmbH & Co. KG, 2022.

[4] T. Wohlers, R. I. Campbell, O. Diegel, R. Huff, and J. Kowen, *Wohlers report 2020: 3D printing and additive manufacturing state of the industry*. Fort Collins, Colo.: Wohlers Associates, 2020.

[5] 3D Hubs B.V., *Additive manufacturing trend report 2021: 3D printing market growth in the year of the COVID-19.* [Online]. Available: https://www.hubs.com/get/trends/ (accessed: Jan. 31 2023).

[6] Sculpteo, *The Sate of 3D Printing: 2022 Edition.* [Online]. Available: https://www.sculpteo.com/de/ebooks/state-of-3d-printing-report-2022/ (accessed: Jan. 31 2023).

[7] Sculpteo, *The Sate of 3D Printing: 2021 Edition.* [Online]. Available: https://www.sculpteo.com/de/ebooks/state-of-3d-printing-report-2021/ (accessed: Dec. 9 2021).

[8] P. K. Mallick, *Fiber-Reinforced Composites*: CRC Press, 2007.

[9] M. Xanthos, *Functional Fillers for Plastics*. Weinheim: Wiley, 2005.

[10] L. J. Tan, W. Zhu, and K. Zhou, "Recent Progress on Polymer Materials for Additive Manufacturing," *Adv. Funct. Mater.*, vol. 30, no. 43, p. 2003062, 2020, doi: 10.1002/adfm.202003062.

[11] T. A. Osswald, *International plastics handbook: The resource for plastics engineers,* 1st ed. Munich, Cincinnati: Hanser, 2006. Accessed: May 17 2022.

[12] P. Eyerer, T. Hirth, and P. Elsner, Eds., *Polymer Engineering: Technologien und Praxis*. Berlin, Heidelberg: Springer Berlin Heidelberg, 2008. [Online]. Available: http://nbn-resolving.org/urn:nbn:de:bsz:31-epflicht-1586329

[13] H. Domininghaus, P. Elsner, P. Eyerer, and T. Hirth, *Kunststoffe*. Berlin, Heidelberg: Springer Berlin Heidelberg, 2012.

[14] L. Jianjun and O. Yuxiang, *Theory of flame retardation of polymeric materials*. Berlin, Boston: De Gruyter, 2019. [Online]. Available: http://www.degruyter.com/search?f_0=isbnissn&q_0=9783110349269&searchTitles=true

[15] L. Lanzl, K. Wudy, S. Greiner, and D. Drummer, "Selective laser sintering of copper filled polyamide 12: Characterization of powder properties and process behavior," *Polym. Compos.*, vol. 40, no. 5, pp. 1801–1809, 2019, doi: 10.1002/pc.24940.

[16] I. Kletetzka, R. Gawlikowicz, and H.-J. Schmid, "Effects of spherical Fillers on the Processability and mechanical Properties of PA613 and PP-based Laser Sintering Dry Blends," in *Proceedings of the 33nd Annual International Solid Freeform Fabrication Symposium*, Laboratory for Freeform Fabrication and University of Texas at Austin, Ed., Austin, 2022.

[17] H. Chung and S. Das, "Processing and properties of glass bead particulate-filled functionally graded Nylon-11 composites produced by selective laser sintering," *Materials Science and Engineering: A*, vol. 437, no. 2, pp. 226–234, 2006, doi: 10.1016/j.msea.2006.07.112.

[18] R. G. Kleijnen, J. P. W. Sesseg, M. Schmid, and K. Wegener, "Insights into the development of a short-fiber reinforced polypropylene for laser sintering," in *AIP Conference*

Proceedings, Lyon, France, 2017, p. 190002. [Online]. Available: https://aip.scitation.org/doi/pdf/10.1063/1.5016791
[19] S. Arai, S. Tsunoda, A. Yamaguchi, and T. Ougizawa, "Effects of short-glass-fiber content on material and part properties of poly(butylene terephthalate) processed by selective laser sintering," *Additive Manufacturing*, vol. 21, pp. 683–693, 2018, doi: 10.1016/j.addma.2018.04.019.
[20] Y. Shi and Y. Zhang, "Simulation of random packing of spherical particles with different size distributions," *Appl. Phys. A*, vol. 92, no. 3, pp. 621–626, 2008, doi: 10.1007/s00339-008-4547-6.
[21] B. O. Sivadas, I. Ashcroft, A. N. Khlobystov, and R. D. Goodridge, "Laser sintering of polymer nanocomposites," *Advanced Industrial and Engineering Polymer Research*, vol. 4, no. 4, pp. 277–300, 2021, doi: 10.1016/j.aiepr.2021.07.003.
[22] K. Wudy, L. Lanzl, and D. Drummer, "Selective Laser Sintering of Filled Polymer Systems: Bulk Properties and Laser Beam Material Interaction," *Physics Procedia*, vol. 83, pp. 991–1002, 2016, doi: 10.1016/j.phpro.2016.08.104.
[23] J. Schmidt *et al.,* "A novel process route for the production of spherical SLS polymer powders," in Cleveland, Ohio, USA, 2015, p. 160011.
[24] R. D. Goodridge *et al.,* "Processing of a Polyamide-12/carbon nanofibre composite by laser sintering," *Polymer Testing*, vol. 30, no. 1, pp. 94–100, 2011, doi: 10.1016/j.polymertesting.2010.10.011.
[25] L. J. Tan, W. Zhu, and K. Zhou, "Development of organically modified montmorillonite/polypropylene composite powders for selective laser sintering," vol. 369, pp. 25–37, 2020, doi: 10.1016/j.powtec.2020.05.005.
[26] F. Baumann and N. Wilczok, "Herstellung von Polyamid-Fällpulvern mit enger Korngrössenverteilung und niedriger Porosität," Patent DE 19708946 A1.
[27] K.-R. Meyer, K.-H. Hornung, and H.-J. Smigerski, "Verfahren zur Herstellung von pulverförmigen Beschichtungsmitteln auf der Basis von Polyamiden mit mindestens 10 aliphatisch gebundenen Kohlenstoffatomen pro Carbonamidgruppe," Patent DE 29'06'647 B1.
[28] Y. Chunze, S. Yusheng, Y. Jinsong, and L. Jinhui, "A Nanosilica/Nylon-12 Composite Powder for Selective Laser Sintering," *Journal of Reinforced Plastics and Composites*, vol. 28, no. 23, pp. 2889–2902, 2009, doi: 10.1177/0731684408094062.
[29] C.-Z. Yan, Y.-S. Shi, J.-S. Yang, and L. Xu, "Preparation and Selective Laser Sintering of Nylon-12-Coated Aluminum Powders," *Journal of Composite Materials*, vol. 43, no. 17, pp. 1835–1851, 2009, doi: 10.1177/0021998309340932.
[30] C. Kummert, W. Diekmann, K. Tews, and H.-J. Schmied, "Influence of Part Microstructure on mechanical Properties of PA6X Laser Sintered Specimens," in *Solid Freeform Fabrication 2019 - Proceedings*, Laboratory for Freeform Fabrication and University of Texas at Austin, Ed., 2019, pp. 735–744.
[31] Sympatec GmbH, *Partikelformanalyse.* [Online]. Available: https://www.sympatec.com/de/partikelmesstechnik/glossar/partikelform/ (accessed: Jan. 31 2023).
[32] *Particle size analysis — Image analysis methods — Part 2: Dynamic image analysis methods*, 13322-2, ISO, 2021.
[33] *Additive Fertigungsverfahren Laser-Sintern von Kunststoffbauteilen Materialqualifizierung*, 3405 Blatt 1.1, VDI, Berlin, 2018.

[34] *Kunststoffe – Dynamische Differenz-Thermoanalyse (DSC) – Teil 3: Bestimmung der Schmelz- und Kristallisationstemperatur und der Schmelz- und Kristallisationsenthalpie*, 11357-3, DIN EN ISO, Berlin, 2018.
[35] *Kunststoffe – Polyamide – Beschleunigte Konditionierung von Probekörpern*, 1110, DIN EN ISO, Berlin, 2019.
[36] *Kunststoffe - Bestimmung der Zugeigenschaften*, 527, DIN EN ISO, Berlin, 2019.
[37] *Kunststoffe – Polyamid (PA)-Formmassen für das Spritzgießen und die Extrusion – Teil 2: Herstellung von Probekörpern und Bestimmung von Eigenschaften*, 16392-2, DIN EN ISO, Berlin, 2017.
[38] *Kunststoffe - Bestimmung von Druckeigenschaften*, 604, DIN EN ISO, Berlin, 2003.
[39] *Kunststoffe – Bestimmung der Wärmeformbeständigkeitstemperatur –Teil 2: Kunststoffe und Hartgummi*, 75-2, DIN EN ISO, Berlin, 2013.
[40] *Kunststoffe – Bestimmung der Wärmeformbeständigkeitstemperatur – Teil 1: Allgemeines Prüfverfahren*, 75-1, DIN EN ISO, Berlin, 2020.
[41] G. W. Ehrenstein, *Polymer-Werkstoffe: Struktur - Eigenschaften - Anwendung,* 3rd ed. München: Hanser, 2011.
[42] J. K. Mackenzie and R. Shuttleworth, "A phenomenological theory of sintering," *Proc. Phys. Soc. B*, no. 62, pp. 833–852, 1949.
[43] L. Benedetti, B. Brulé, N. Decraemer, K. E. Evans, and O. Ghita, "Evaluation of particle coalescence and its implications in laser sintering," *Powder Technology*, vol. 342, pp. 917–928, 2019, doi: 10.1016/j.powtec.2018.10.053.
[44] J. Frenkel, "Viscous flow of crystalline bodies under the action of surface tension," *J. Phys.*, no. 9, pp. 385–391, 1945.
[45] I. Kletetzka, M. Kosanke, D. Meinderink, V. Neßlinger, G. Grundmeier, and H.-J. Schmid, *Influence of the filler matrix adhesion and the effects of conditioning on tensile properties of laser sintered parts built with polyamide glass bead dry blends*, 2023.
[46] *Metallische Werkstoffe - Zugversuch*, 6892, DIN EN ISO, Berlin, 2020.